



Control of Carbon Dioxide Sequestration by Mechanical Activation of Red Mud

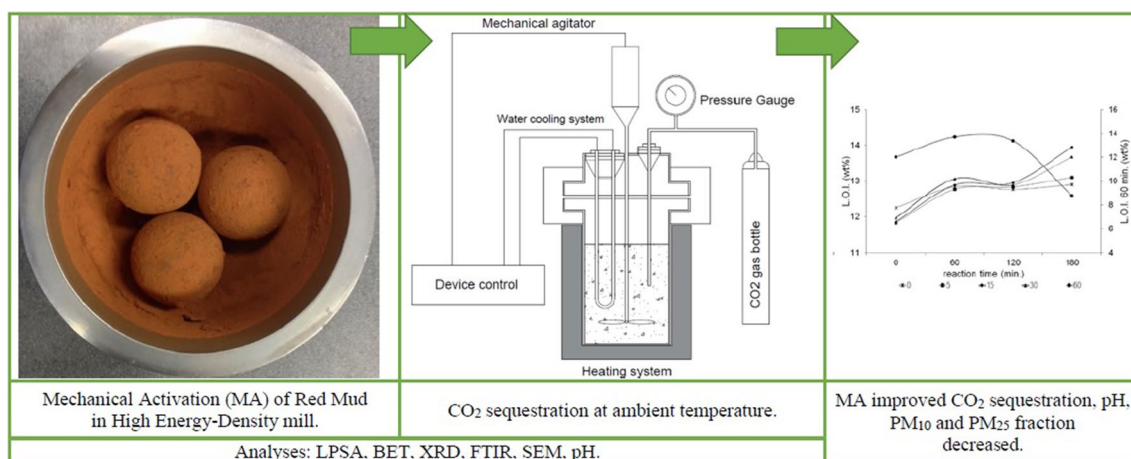
Gábor Mucsi¹ · Nóra Halyag¹ · Tamás Kurusta¹ · Ferenc Kristály²

Received: 2 July 2020 / Accepted: 30 April 2021 / Published online: 15 May 2021
© The Author(s) 2021

Abstract

Mineral carbonation is a potentially attractive sequestration technology for the permanent safe disposal and immobilization of CO₂. In this technology, CO₂ is chemically reacted with calcium, sodium, and magnesium containing materials to form thermodynamically stable and environmentally harmless minerals, usually carbonates. In our research, mechanical activation of red mud was carried out in order to enhance its reactivity by means of mechanochemical reactions (surface activation), and its sequestration behaviour was investigated using carbon dioxide gas at 25 °C temperature and at high pressure (5 bar) in an autoclave. The reacted red mud was characterized by Fourier-transformed infrared spectrometer, scanning electron microscopy, X-ray diffraction, laser particle size analyzer, BET specific surface area measurement, and pH measurement. It was found that mechanical activation improved the CO₂ sequestration ability by 1.7 wt% of red mud, as demonstrated by the above investigations. The pH of red mud slurry can be lowered by reacting it with carbon dioxide. During our measurements, the pH of the suspension decreased from 10 to 6.81. Furthermore, the carbonation process can be successfully used to decrease the amount of harmful PM₁₀ (particles with a diameter of 10 μm or less) and PM_{2.5} (particles with a diameter of 2.5 μm or less) fraction. The proportion of 10 μm particles can be reduced by 40% and that of 2.5 μm by 20%.

Graphic Abstract



Keywords Red mud · Mechanical activation · CO₂ sequestration · Material structure · Waste utilization

Statement of Novelty

Based on the literature survey, it was concluded that authors reported about different types of waste materials and commercially available primary material resources

✉ Gábor Mucsi
ejtmucsi@uni-miskolc.hu

Extended author information available on the last page of the article

for CO₂ sequestration. However, till date no such literature is available on the utilization of mechanically activated red mud for CO₂ sequestration. The hypothesis was to tailor the reactivity (carbonation) of red mud prior to CO₂ sequestration by surface activation. Therefore, our research aim was to investigate the effect of mechanical activation of red mud on the CO₂ sequestration behaviour and find correlation between the grinding parameters and the microstructural properties of the resulted carbonate bearing material.

Introduction

Increasing CO₂ emission which accelerate global warming, is one of the major global environmental issues. In order to reduce CO₂ footprint there are several techniques developed for its sequestration and capturing. Geological sequestration, disposal into the ocean, and biological fixation are widely investigated. Mineral carbonation is one of the most promising method, with ever increasing experiments and applications of CO₂ fixation in basalts or waste materials. Mineral carbonation is a reaction of CO₂ with non-carbonate minerals: or wastes to form geologically and thermodynamically stable forms of carbonates [1–3] of the natural rocks, olivine-rich mafic and ultramafic rocks can be used for CO₂ sequestration [4].

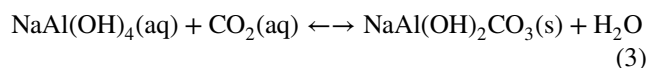
Nowadays, the most commonly used materials for CO₂ sequestration are soils [5], steel slags [6, 7], fly ash [8], amine solutions, zeolites, porous membranes, serpentine, olivine [9–11], cementitious materials [12], construction and demolition waste [13, 14], metal–organic frameworks, deep geological strata [15] and red mud [3, 16]. An optimal field among the possible techniques is the application of industrial wastes as sequestration media. Red mud as the waste of alumina production from bauxite, can be used as a material to capture and storage of anthropogenic CO₂, mainly as near-source capture for fossil fuel power plants [17], cement factories, foundries, and metal-working plants.

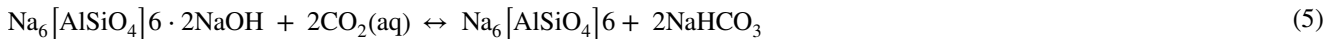
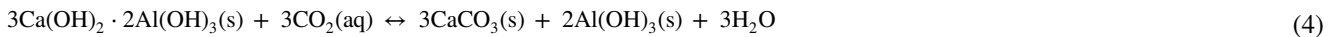
After bauxite digestion in the Bayer process, a large amount of highly alkaline (pH > 11) thixotropic, fine-grain insoluble suspension remains, with red color and variable mineralogical and chemical composition. The main components of red mud are Fe₂O₃ (30–60 wt%), Al₂O₃ (10–20 wt%), SiO₂ (3–50 wt%), Na₂O (2–10 wt%), CaO (2–8 wt%), and TiO₂ (trace-10 wt%) [18]. The production of 1 ton of alumina generates 1–1.5 tons of red mud [19]. From the globally generated red mud only 3–4% is re-utilized, while the remaining amount remains stored in drying ponds.

The disposal of such a large quantity of alkaline sludge is expensive due also to its hazardous nature posing several environmental risks: the high pH (11–13), high Na concentration (~ 50 g/kg), and very fine particle size (90% under then 10 μm). The elevated pH makes red mud a caustic, highly corrosive material, possible source of severe accidents. Pond-base exfiltration into the basement may lead to Na-contamination of groundwater resources and soils. The fine grain size leads to atmospheric contamination in the PM10 value by dusting on the drying surfaces. Related to physical properties arises also the major barrier in the re-utilization of red mud: the high bound water content which rises the costs if it has to be evaporated prior to beneficiation.

To reduce the problem of accumulating large amounts of red mud, several disposal techniques have been investigated [20]. Neutralization by forced carbonation of NaOH with added carbon-dioxide [21] shows the greatest potential to provide sustainable outcomes. Furthermore, saline brine or seawater [22], Ca and Mg-rich brines, soluble Ca and Mg salts, acidic water from mine tailings, fly ash, and carbon-dioxide gas [6], has the neutralization potential through carbonation which reduces causticity. Based on literature data the re-utilization of red mud can be divided into three categories: construction, metal recovery, and neutralization. The disposed red mud after neutralization can be applied in the production of building materials such as bricks [23], ceramics [24, 25], glazes, pigments, paints, tiles [26], cement additive and paving tiles [27, 28, 29, 30, 31, 32, 33, 34] and as stabilization material for clay liners [35, 36]. In some cases it serves as soil amendment [37] and fertilizers [38]. More sophisticated fields are red mud-polymer composite panels as wood substitute [39], geopolymers [40, 41], iron rich cement [42], radiopaque materials [43]. It might be also disposed as road base material [44] and in sewage treatment [45, 46] as sorbent for removal of lead, chromium, arsenic [19, 46–50], fluoride [18, 50–59], cadmium, zinc [60] from aqueous solutions. Applications for CO₂ sequestration of industrial emissions were also tested [21]. Recovery of trace metals as V, Cr, Ti, and rare-earth elements is also possible beneficiation for some red muds [30].

The neutralization of aqueous red mud solution takes place by the following carbonation reactions of CO₂ [6]:





The carbonic acid formed in the CO₂ bearing fluid neutralizes the bases and precipitates as sodium, calcium, and magnesium carbonates. For the aqueous carbonation process, irreversible hydration of calcium oxide is followed by simultaneous dissolution of Ca(OH)₂ and dissociation of aqueous CO₂ and precedes the carbonation reaction. As the Ca²⁺ ions are converted to CaCO₃ and precipitated, more Ca(OH)₂ dissolves to equalize the Ca²⁺ concentration. In the aqueous carbonation of silicate bound Ca and Na, the first step is CO₂ dissolution in the aqueous phase producing H⁺ ions. In the resulting slightly acidic environment Ca (Mg) and Na leaches from the silicate matrix, and the system proceeds to carbonate precipitation. The rate and extent of cation leaching were found to be inversely related to particle size and pH and increased with higher temperature, pressure, and specific surface area. The extent and rate of carbonation depends on the diffusivity and reactivity of CO₂ controlled by porosity and physical conditions (partial pressure, relative humidity, temperature, and pressure). According to Huntzinger et al. [61], Huijgen et al. [62], Uibu et al. [63], and Kuusik et al. [64], the main mechanism affecting the rate and extent of carbonation are transportation-controlled mechanisms such as CO₂ and Ca²⁺ ions diffusion to/from reaction sites, boundary layer effects (diffusion across precipitate coatings on particle surface) dissolution of Ca(OH)₂ at the particle surface and pore blockage/coating. The main products of slurry forced carbonation are Na₂CO₃ and NaHCO₃. Soluble Na-carbonates provide less permanent CO₂ storage than solid Ca-Mg-carbonates because of their solubility. As dissolved NaOH is enriched in surface layers of the ponds [65] precipitation of Na-carbonates through drying is favored, but rehydration will remove these solid phases.

Several studies proved that mechanical activation of various minerals and secondary raw materials improved the CO₂ sequestration capacity [66, 66, 67, 67, 68] by increasing material fineness and generating amorphous layers on grain surfaces, crystallite size reduction, and micro-strain accumulation resulted in enhanced reactivity of solids. One of the major components of red mud is cancrinite [69], a tectosilicate which contains additional anions, most frequently CO₃[−], OH[−], Cl[−] and SO₄ [70]. If ratio of OH[−] increases precipitation of hydroxyl cancrinite is possible. Since cancrinite structure has anion exchange capacity and is able to crystallize in low temperature hydrothermal conditions in highly alkaline environment, it could be expected to be involved in carbonation reactions.

Based on the above introduction experiments were conducted on different types of waste materials and commercially available primary materials for CO₂ sequestration. However, till date no such literature is available on the utilization of mechanically activated red mud for CO₂ sequestration. Grinding work was against the binding energy of crystalline materials. The internal energy of a unit mass dispersed system is the sum of the binding energy and the surface energy of the system. Grinding as a mechanical activation can be characterized by a change in the binding energy [71]. The hypothesis was to enhance the reactivity (carbonation) of red mud prior to CO₂ sequestration by surface activation. Therefore, our research aim was to investigate the effect of mechanical activation of red mud on the CO₂ sequestration behaviour and find correlation between the grinding parameters and the microstructural properties of the resulted carbonate bearing material.

Materials and Methods

Materials

Red mud used in this study was acquisitioned from Almásfüzitő red mud repository. Initial moisture content of 38.16 wt% and particle density of 2.69 g/cm³ are specific. Grain size distribution analysis shows 0.4–13 μm with the median size d₅₀ = 2.37 μm and 31,400 cm²/cm³ geometric and 28.44 m²/g BET actual specific surface area. Hematite (21%), cancrinite (17.7%), and goethite (28.5%) are the major phases identified in the red mud by XRD measurement. Several accessory minerals were also identified (gibbsite, calcite, hydrogarnets), and the amount of amorphous phase was 13.4 wt%. For the sequestration tests research grade (99.5%) Biogon C CO₂ gas was used without further purification.

Sample notation scheme was set up as “AV-I.5.60” in which “AV_I” means Almásfüzitő red mud, “5” is grinding time in minutes, and “60” is the carbonation reaction time in minutes.

Methods

Mechanical Activation

The raw red mud was dried in a laboratory oven at 105 °C till constant weight. Mechanically activation was done by grinding in a Retsch planetary mill for 5, 15, 30, 60 min. Each milling stage was produced on a new batch of raw red mud. The

mill speed was set to 128 rpm, and the grinding ball diameter was 40 mm. The ground material was later investigated with laser particle size analyzer and FTIR measurements.

CO₂ Sequestration Experiment

The mineral carbonation reactions were performed in a Parr high-pressure- and temperature-controlled autoclave that with the active volume of 0.3 dm³. Suspension was prepared by mixing red mud with distilled water at 0.3 L/S ratio (3.33 g/L) to obtain a sufficient volume of slurry for carbonation reaction and the back-pressure regulator controlled the system pressure.

Experiments were carried out at 5 bar pressure with continuous mixing. To ensure the sufficient amount of CO₂, the red mud slurry was set to fill up 70% volume of the reaction vessel. The applied process parameters were 25 °C temperature, and 1, 2, 3, and 4 h reaction times, with 245 1/min revolution number of stirrer.

Pressure was applied to increase CO₂ dissolution in the fluid expecting enhanced carbonation reactions. Slight decrease of pressure with time was observed, due to the consumption of CO₂ by carbonation. In order to ensure the CO₂ necessary for the reaction we have refilled the amount of gas required to achieve the initial pressure every 15 min. The variation of pH was measured before and after reaction with a digital pH meter. The high pH before reaction is caused by the NaOH in the Bayer-process liquor. The carbonated samples were dried in a laboratory oven to carry out analytical measurements (FTIR, SEM, XRD). The particle size distribution of the reacted samples was measured after reaction immediately in wet state by laser particle size analyzer.

Characterization

Particle Size Analysis

The particle size distribution of the raw and ground red mud was measured by HORIBA LA-950V2 laser particle size analyzer in wet mode by using distilled water as dispersing media. This measurement was carried out after the carbonation reaction also. For better dispersion of fine particles, before the measurement, sodium pyrophosphate was added, and it was measured under ultrasonic stirring for one minute. Particle size distribution was calculated based on the Mie-theory with the red mud refractive index.

Mineralogical Characterization by X-ray Diffraction

The mineralogy of the red mud sample before and after CO₂ sequestration was determined by X-ray powder diffraction (XRD) with a Bruker D8 Advance diffractometer using Cu K-alpha radiation (40 kV, 40 mA) in parallel beam geometry obtained with Göbel mirror, in the 2°–70° (2θ) range with a 0.007° (2θ) step interval and a 24 s step counting time. The crystalline phases were identified by Bruker *DiffracPlus* software package in its EVA module ICDD PDF-2 (2005) database for search/matching of phases. The quantitative evaluation was carried out by Rietveld refinement in TOPAS4 software, where the amorphous content was determined by the amorphous hump method.

Fourier Transformed Infrared Spectroscopy

Stretching and bending vibrations of chemical bonds in the samples before and after CO₂ sequestration was detected by a JASCO FT-IR 4200 type Fourier Transformed Infrared Spectrometer in reflection mode with a diamond ATR. The infrared transmission spectra of samples were recorded for 400–4000 cm⁻¹ with the resolution of 4 cm⁻¹. The observed spectra are plotted in the function of wavenumber and transmittance. The interpretation of observed FTIR bands was done based on the handbook by Chukanov and Chervonny [72].

Scanning Electron Microscopy

Scanning electron microscopy (SEM) was used to take images of the samples for visual observation of particle size, surface morphology, and formation of new phases. The back-scattered images (BSE) were taken with a Phenom ProX Desktop SEM instrument with ×6900 magnification under 15 kV voltage. Additionally, energy dispersive X-ray spectrometry (EDX) was used to study the chemical composition of the samples.

BET Specific Surface Area Measurement

For the measurement of the total specific surface area of samples a Micromeritics Gemini VII apparatus was used. Each sample was degassed before the measurement. The gas used for adsorption was nitrogen. The specific surface area was calculated by a 5-point BET method.

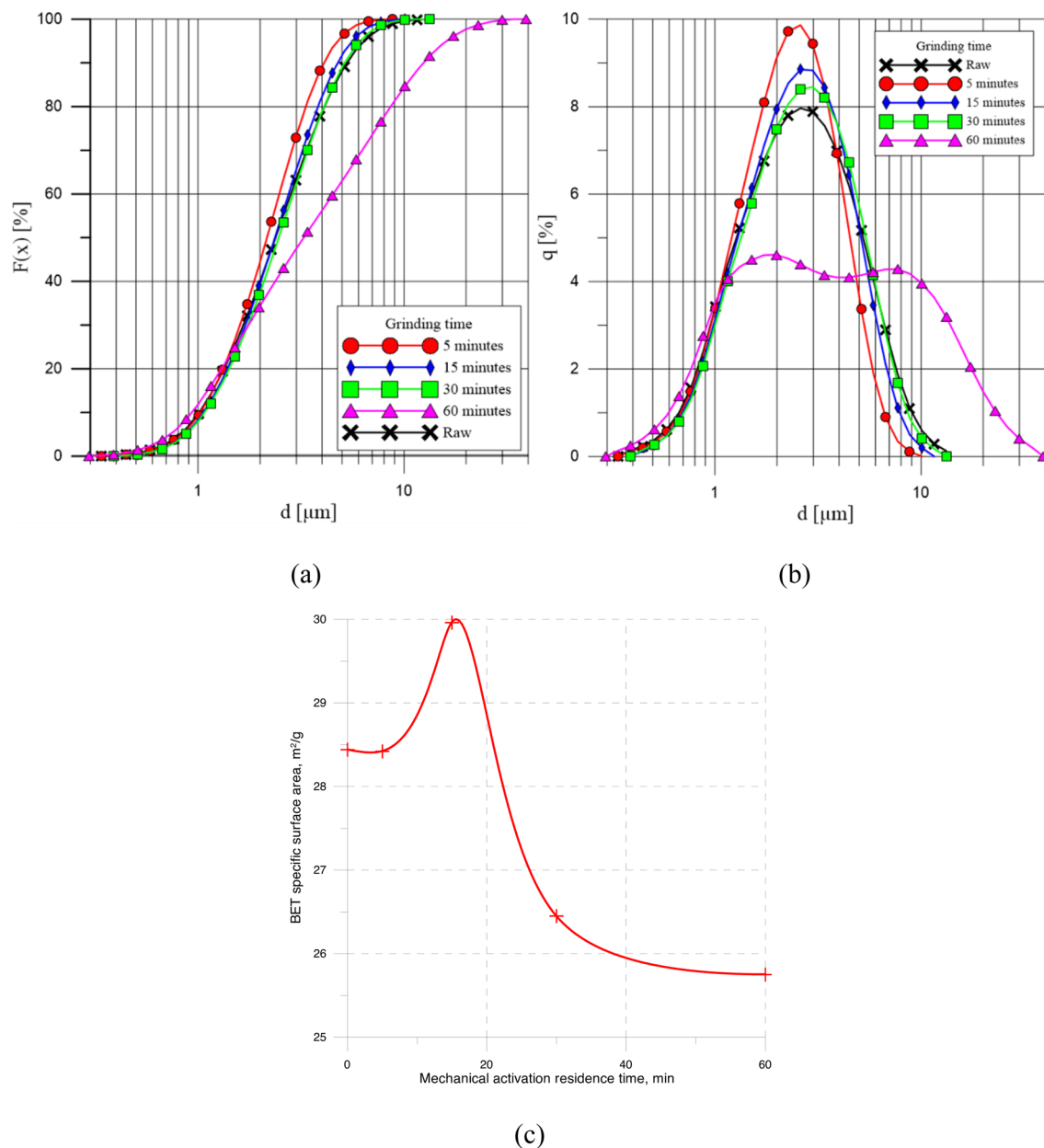


Fig. 1 Particle size distribution (a) and frequency distribution (b) curves of the raw and ground red mud sample, (c) BET specific surface area of the raw and mechanically activated red mud and

Results and Discussion

Mechanical Activation of Red Mud

Particle Size Distribution and Specific Surface Area

The aim of mechanical activation by grinding was to increase and activate the particle surfaces on which the carbonation reactions take place. The increased SSA and amorphization of particle surfaces is beneficial to enhance

carbonation reactions. Based on the particle size distribution (Fig. 1a, b) the amount of the coarse fraction changed slightly in each case except for 60 min grinding where a significant increase can be observed. The sample milled for 5 min had the finest particle sizes with narrow distribution. On the frequency distribution curve (Fig. 1b) the amount of fraction between 1.7 and 4.5 μm started to increase after 5 min grinding, then further grinding shifted the distribution to higher size fraction with parallel decrease of specific surface area due to the aggregation of particles.

The results show that the highest BET specific surface area can be reached by grinding after 15 min, the specific surface area of the initial raw material increased from 2828.44 up to 2929.96 m²/g (Fig. 1c). The grinding for 55, 30, and 60 min decreased the specific surface area down to 28.42 m²/g, 26, 26.45 m²/g, and 2525.75 m²/g respectively due to aggregation/agglomeration. These results are not quite well correlated with the particle size distribution of the ground red mud. The particle size decreases in the first 15 min, the geometric surface area and particle sizes indicate the tendency of the powder to form agglomerates due to prolonged milling. However, these agglomerates contain meso- and macro pores, which are of great importance in surface reactions. The pores in relatively weaker (soft) agglomerates remain accessible for nitrogen, thus BET results describe more closely the actual SSA.

Structural Characterization of the Red Mud by FTIR

The FTIR spectra of the mechanically activated red mud samples (by grinding) is shown in Fig. 2, showing that band positions and symmetry of the raw and ground material were not changed. However, differences were observed in their intensities, the decreasing transmittance values indicating the aggregation of fine particles, the same process being observed by PSA (Fig. 1a, b). The H₂O and OH stretching region of 3300–3000 cm⁻¹ shows the presence of OH (in silicates and goethite) and strongly bound water in mesopores [73]. The peak at 2360 cm⁻¹ could be attributed to the H–O–H group of weakly bound water [74], which disappears upon drying after CO₂ sequestration. By milling, this absorption region and the 1640 cm⁻¹ is decreasing in intensity, supporting the presence of water which was not removed by 105 °C drying and is mostly contained in

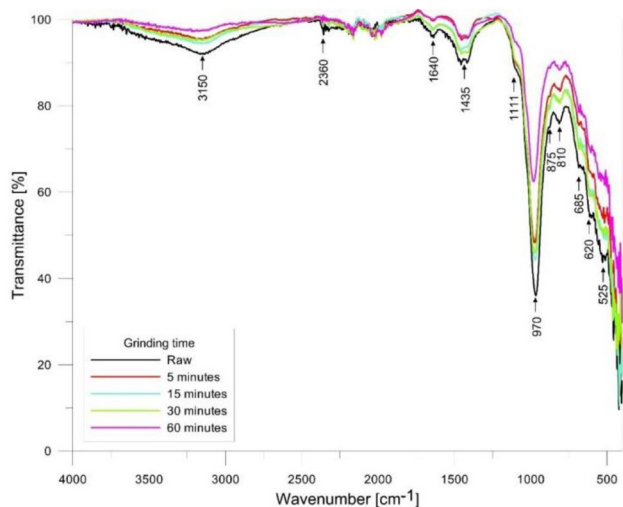


Fig. 2 FTIR spectra of the ground red mud sample

goethite [75]. However, H₂O in cancrinite is also producing bands in the 1630–1650 cm⁻¹ region [76].

Part of the strongly bound water and also OH groups is supposed to be contained in the amorphous phase. The presence of carbonate groups is confirmed by strong asymmetric C–O stretching vibration in the 1420–1450 cm⁻¹ region, with double maximum centered at 1435 cm⁻¹ [74]. These values together with the medium sharp C–O bending at 875 cm⁻¹ indicate the presence of calcite, but carbonate groups of cancrinite have a series of weak bands in the 1390–1490 cm⁻¹ region. The peaks at 1000–1120 cm⁻¹ indicate the asymmetric stretching of Si–O–Al framework (cancrinite, hibschite) but also O–Fe–O for goethite. The peaks at 970 cm⁻¹ are due to the presence of Si–O–Si(Al) bonds. Smaller peaks were observed in the region of 685 cm⁻¹ due to the symmetric stretching of the Si–O–Al framework. The peak at 525 cm⁻¹ caused by the Fe–O bond. At wavelengths of 1000–1120, 970, 685, and 525 cm⁻¹, typical bands characteristic for red mud minerals are seen [77]. With enhanced grinding time similar decrease in the intensity can be observed in the 1435 cm⁻¹ carbonate (calcite) band, and 970 cm⁻¹ Si–O–Si(Al) bands. The most significant intensity decrease can be observed in the 60 min milled sample. The decrease of transmittance is due, beyond aggregation of fine particles, to the amorphization of particle surfaces.

Carbon Dioxide Sequestration

Particle Size Distribution

Particle size measurements were carried out to observe how particle sizes from different grinding times varies with the same reaction time, depending on the SSA. The variation in particle size is influenced mainly by two circumstances: (1) coarsening due to cementation of particles by carbonate coating, (2) particle decrease by digestion and dissolution upon longer reaction times. Digestion is a part of the process which produces new reaction surfaces. Therefore, changes in particle size distribution are one of the indicators of surface reactions.

During the first 1 h of reaction time the particle size distribution curve shows an increase which may be the result of carbonate cementation of particles (Fig. 3a). This carbonate layer seems to cover the particles equally as proved by the shift of the curve to coarser sizes.

In the second experimental set with 2 h of reaction time (Fig. 3b) the particle size increased depending on the grinding time. The highest coarsening was reached with 15 min grinding. This may be the result of micro cracks (highest BET specific surface area) of the particles due to grinding, in which the dissolved CO₂ can react with the silicates present in the red mud. The particle size of the 30 min milled material did not change significantly that may be the result

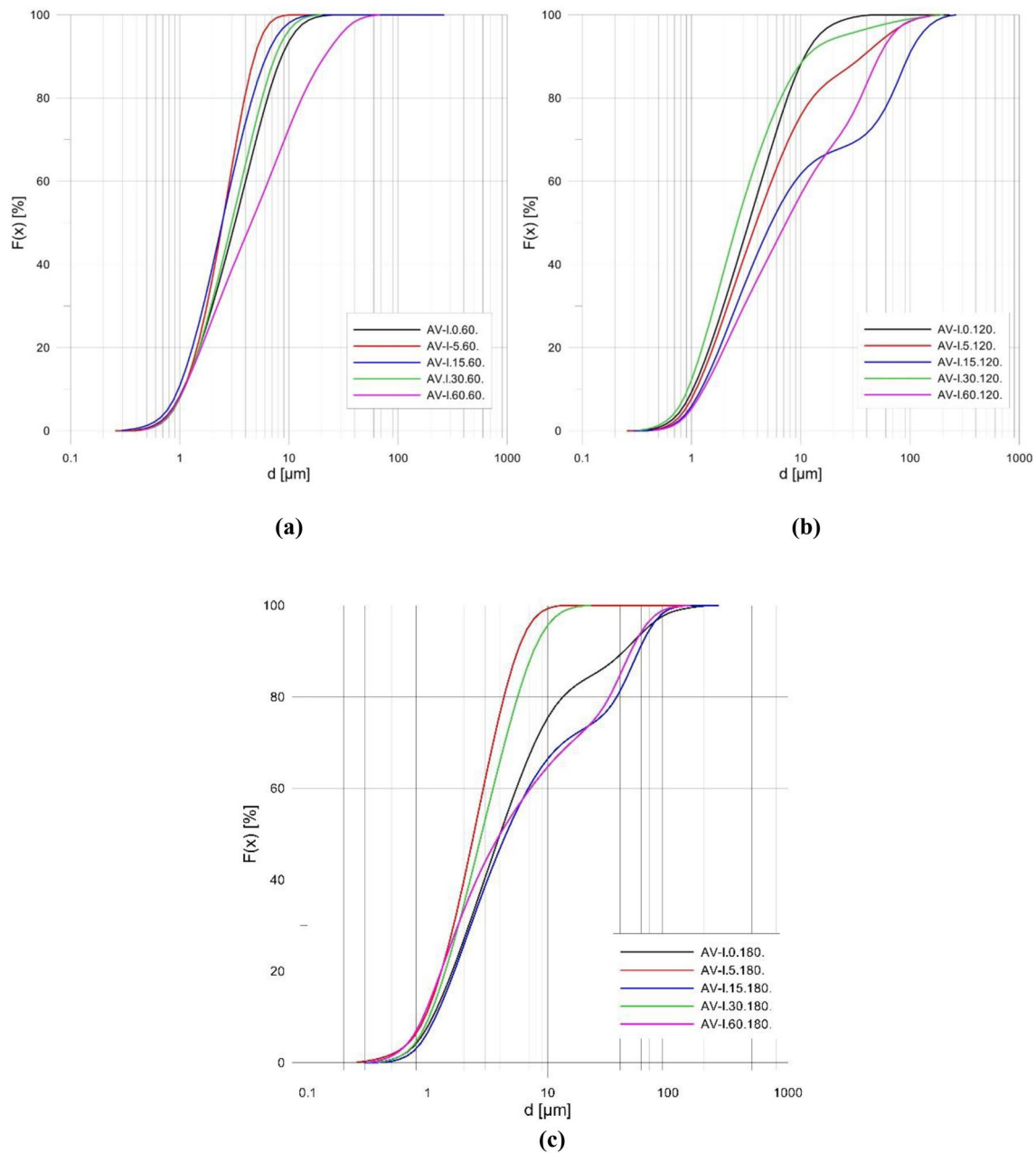


Fig. 3 Particle size distribution curve after 60 min (a), 120 min (b) and 180 min (c) reaction time (0, 5, 15, 30 and 60 min grinding time)

of the clogging of the previously formed cracks that reduced the reaction surface. In the experiment with 3 h reaction time no trend was found in the variation of the particle size distribution (Fig. 3c) due to the multiple variation in dissolution–reprecipitation of formed carbonate bearing materials.

The variation of median particle size (d_{50}) at various grinding times is also responding to the CO_2 fixation. It is noted that the most significant difference was found at 60 min milled sample, where d_{50} increased from 3.33 to 7.34 μm (120 min reaction time) and decreased again to 4.01 μm (180 min reaction time). The lowest variation in

particle size was found at the 30 min mechanically activated red mud after sequestration which has one of the lowest BET surface area and second coarsest median particle size. The maximum value of the median particle size was reached at 120 min residence time of CO_2 sequestration, except of raw red mud where continuous increase was detected.

Concentration of particulate matter (PM) in air is an important issue from environmental point of view in Europe as well as worldwide (Air quality in Europe, 2017). Two important factors are the PM_{10} and $\text{PM}_{2.5}$ which means

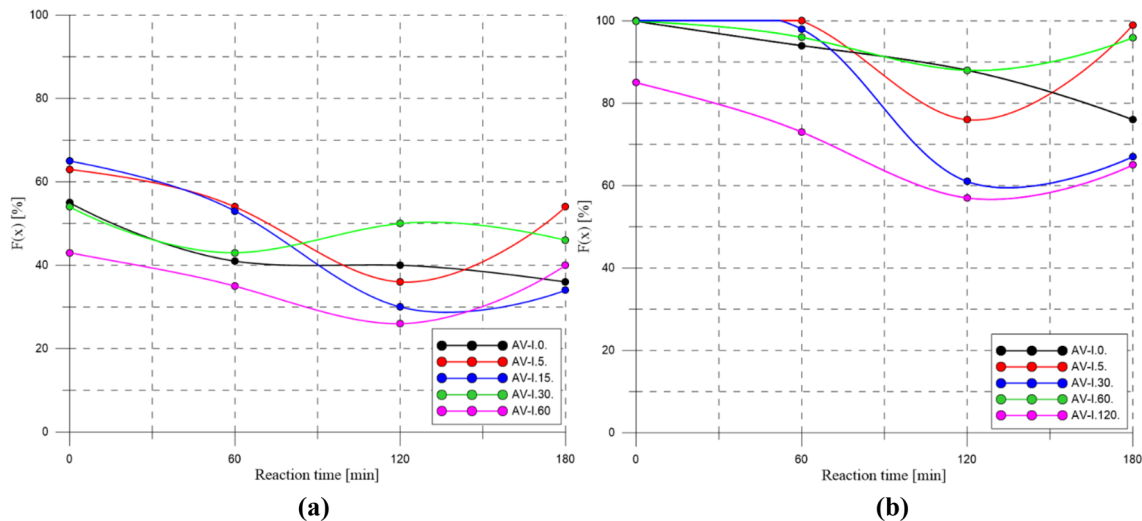


Fig. 4 The amount of $PM_{2.5}$ (a) and PM_{10} (b) as function of reaction time and mechanical activation residence time

particulate matter below 10 μm and 2.5 μm particle size respectively. Since red mud is a very fine material its dusting is a risky characteristic, therefore it is important to see how the CO_2 sequestration change the particle size of red mud particles (Fig. 4).

The initial material was nearly 100% below 10 μm particle size. After 60 min. CO_2 sequestration residence time this size fraction decreased to 85%. In the first 60 min. the AV-I.5. does not contain the size fraction above 10 μm that may be the result of large SSA that was covered equally with the thin carbonated layer. The agglomerated particles with coarser size produce bigger particles after carbonation as proved the AV-I.60 sample. The 60 min reaction time is further and significantly reducing the finer than

10 μm fraction, which is the result of enhanced carbonate formation. This was the reaction time where the highest CO_2 sequestration values were obtained from this point of view. In the 180 min residence time there is slight decrease in particle size, which is probably due to the dissolution of carbonated particles. For $PM_{2.5}$ size fraction (< 2.5 μm) for the first 60 min, the curves are like that of the PM_{10} size fraction (< 10 μm) except for the initial deviation from grinding. The 120 min carbonation residence time reduced most significantly the proportion of particles below 2.5 μm , but the material of the AV-I.30 sample has already begun to dissolve.

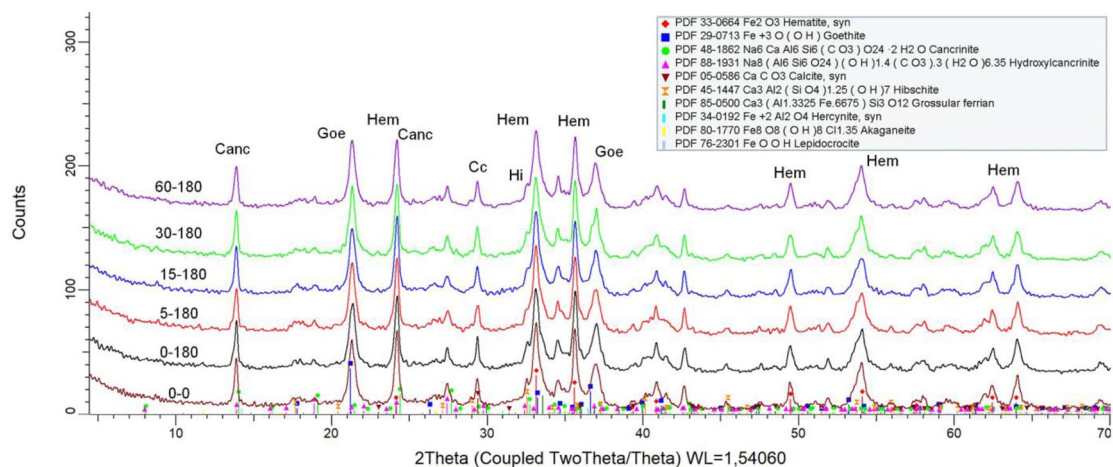


Fig. 5 X-Ray diffraction pattern of the raw red mud and after mechanical activation and after carbon dioxide sequestration sample, the minerals identified by the Search/ Match algorithm

Table 1 The results of the quantitative evaluation (wt%, error ± 1 relative%) of XRD on raw red mud and after mechanical activation and after carbon dioxide sequestration

Phase name	Grinding-time (min)—reaction time (min)					
	0–0	0–180	5–180	15–180	30–180	60–180
Hematite	21.0	19.9	20.0	19.0	18.5	17.2
Goethite (Al)	28.5	28.0	24.7	29.9	27.4	28.0
Calcite	3.2	2.7	3.8	3.4	3.9	3.4
Cancrinite (OH)	17.7	17.7	17.0	15.6	11.8	14.5
Gibbsite	3.7	1.4	5.3	5.3	4.4	4.2
Grossular (Ca,Fe)	2.6	0.7	1.3	0.9	0.5	0.3
Hibschite	8.0	7.2	4.6	5.3	4.5	4.7
Cancrinite (OH,CO ₃)		1.3	2.7	2.2	6.0	4.5
Hercynite	1.4	4.6	4.2	4.6	2.7	3.1
Lepidocrocite	0.5	0.4	0.4	0.3	0.5	0.2
amorphous	13.4	16.0	16	13.5	19.7	19.7

Chemical composition of the phases is shown in Fig. 5

Based on the above results, precipitation from the solution during the first two hours was dominated, followed by dissolution resulting in the reduction of particle size.

Structural Characterization of the CO₂ Sequestered Material by X-Ray Diffraction

Changes in the RM composition (Fig. 5 and Table 1) the main components of red mud are hematite, gibbsite, and cancrinite. However, the sample does not contain detectable amounts of titanium minerals (anatase, rutile), which several researchers have described [26, 78]. This is presumably due to how the mud is classified by density after it is placed in storage. Due to its density, the titanium phase is placed at the bottom of the pitfall [79]. An increase of amorphous content is the result of the mechanical activation by grinding, which is related mostly to the hematite content decreasing continuously with grinding time. It is important to note that slight change in amorphous content might be the indicator of surface activation which is one of the states of mechanochemical reactions [80]. Regarding the CO₂ reacted samples the peaks of cancrinite developed an asymmetry (shoulder) indicating a change in cancrinite composition. This observation is in contrast with Yadav et al. [3] who observed that cancrinite decomposes into nepheline, calcite and water under the action of CO₂ reaction. However, their experiments did not involve mechanical activation, only chemical reactions. The composition of the applied RM was also different, containing chantalite, CaAl₂SiO₄(OH)₄. Since the chantalite major peaks in XRD are overlapping with goethite (~21°2Th), calcite (~29.5°2Th) and hematite (49.5°2Th) as comparing with our results, we cannot identify chantalite in our samples, nor decide if identification by [3] was done correctly. On the other hand, minerals identified in our samples are well in the type and range for most common red mud components, according to Reddy et al. [81].

In order to solve the measured patterns, a cancrinite structure related to carbonate bearing variety was introduced in the Rietveld refinement, applying C to OH substitution and fitting the unit cell parameters. In this way, an increasing amount of carbonated cancrinite was detected with increasing reaction time. Hibschite, a hydroxyl bearing garnet, was also decreasing in the reacted samples, due to the reaction with CO₂ and Na from amorphous material, and probably resulting in carbonated cancrinite also. An increase in gibbsite concentration can be observed similarly to the work of Ramesh et al. (2010). This increase in concentration can be related to the carbonate conversion of hibschite. This transformation is described by [82] with another member of the hydrogrossular group with the katoite. It improved the dissolution of hibschite with mechanical activation, which is consistent with that described by [83].

The sequestration of CO₂ in solid phase must lead to increase in weight of the samples. On the other hand, CO₂ will be liberated upon high temperature calcination from any mineral structure. Based on these facts, in order to control the CO₂ capture of samples, we conducted loss on ignition (L.O.I.) tests at 950 °C, with 15.8 °C/min heating rate and 90 min residence time.

The recorded L.O.I. values (Fig. 6b) correlated well with the CO₂ capture and subsequent weight loss, except for the material milled to 60 min, in this case it increased by 1.6 wt% after a reaction time of 60 min, then decreased to 1.4 wt% after 120 min and reacted to – 3.2 wt% after 180 min. A similar dropping trend is observed for the 15 and 30 min milled material at 180 min reaction time, indicating that agglomeration of particles starts at 15 min grinding and is inhibiting CO₂ sequestration. Basically, it can be established that increased L.O.I. value compared to the initial data due to the CO₂ sequestration on mechanically activated red mud proved the carbonation reactions. The best results were

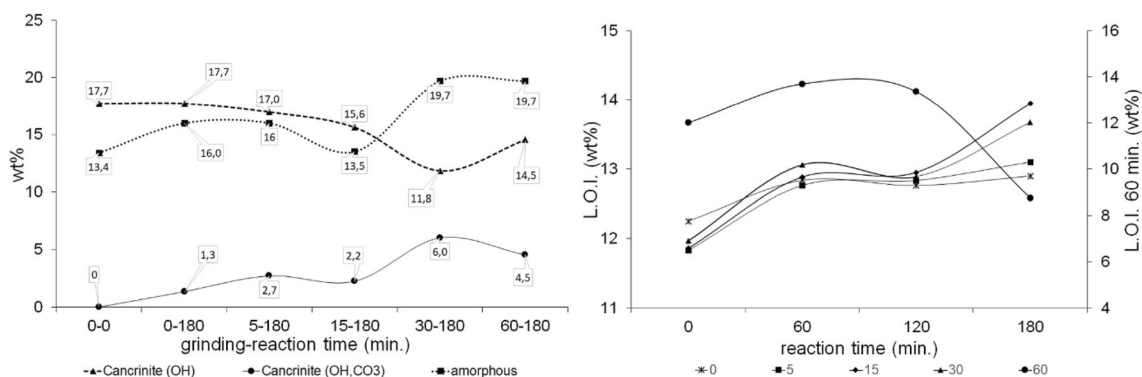


Fig. 6 **a** The effect of reaction time on the amount of Cancrinite in ground red mud and amorphous phase; and **b** the relation of reaction time to the L.O.I. on ground and CO₂ sequestered red mud

obtained with a grinding and reaction time of 60 min, in which case the sample contained 1.6 wt% carbonate.

In this way, 16 g/kg of CO₂ can be isolated, which is 12 g more than in the case of ophiolite [84] and 6 g more than mechanically, and 6 g more than can be sequestration on mechanical activated olivine-basalt [4].

Structural Characterization by FTIR Spectroscopy

The FTIR investigation of the carbonated red mud samples helps to understand their CO₂ sequestration ability. The positions of the absorption bands are nearly similar. The changes in transmittance of CO₃²⁻ group bands can be observed in the carbonated sample. Figure 7a–c show the FT-IR spectra of raw red mud and neutralized red mud (NRM). The 875 cm⁻¹ band belongs to calcite, while the 833 cm⁻¹ band of hibschite is shifted to ~810 cm⁻¹, due to Ca-Fe substitution. The strong bands in the 900–1200 cm⁻¹ region belong mainly to the cancrinite structure, especially important is the 1100 cm⁻¹ band, showing the presence of OH⁻ and CO₃²⁻ cancrinite structure types. The change in intensity and position of this band supports the observations by XRD, the development of carbonate bearing cancrinite. The band at 2160 cm⁻¹ confirmed that the fresh red mud captured CO₂ from the atmosphere, however through molecular absorption and not carbonation. The 1420–1450 cm⁻¹ bands indicate the stretching vibrations of C=O, show the presence of carbonate groups, 1427 cm⁻¹ for calcite and 1400 for carbonate cancrinite. This is due to chemisorbed CO₂ and carbonate formation in fresh red mud, and since calcite amount is relatively stable according to the XRD, the variation of band position and intensity of this region is also related to cancrinite carbonation. Chukanov et al. [76] reported overlapping bands at 1396, 1444 and 1489 cm⁻¹

for a hydroxycancrinite-cancrinite transitional mineral phase. Values of 1381, 1397, 1434, 1480 and 1512 cm⁻¹ are reported by Ventura et al. [85]. Combined with the data from Chukanov and Chervonnyi [72] one observes that carbonate vibrations in cancrinite structure are complex and unique for each sample, although a common region can be delimited.

After 60 min reaction time (Fig. 7a) the mechanically activated samples show slightly more intense carbonate bands at ~1435 cm⁻¹ indicating carbonate fixation. The 5 min milled sample shows the most intense band, which may be the result of higher specific surface area in which the carbonate layer formed. A further slight decrease occurs as a function of increased grinding time.

The 120 min CO₂ residence time decreased the transmittance of AV-I.5 and AV-I.30 sample indicating decrease in carbonation (Fig. 7b) in accordance with the previously presented particle size analyses. The dissolution begins after this 120 min reaction time.

The 180 min reaction time (Fig. 7c) shown the most intense carbonate peak in the case of 15 min grinding which is well correlated with the L.O.I. values (Fig. 6b). The 5 and 30 min. milled samples had similar transmittance supporting the role of particle size distribution, in carbonation, through available activated surface. The lowest amount of carbonates remained in the samples ground for 60 min and in the raw red mud sample. Based on the measurements, according to the carbonate band characteristics, the 15 min mechanically activated samples gave the best results, which required a 180 min reaction time.

Based on the measurements, it was observed that the samples reached a maximum point in the amount of captured CO₂ followed by a decrease instead of stabilization which shown fluctuation. The evolution of OH and H₂O content of red mud phases is also responding to mechanical activation

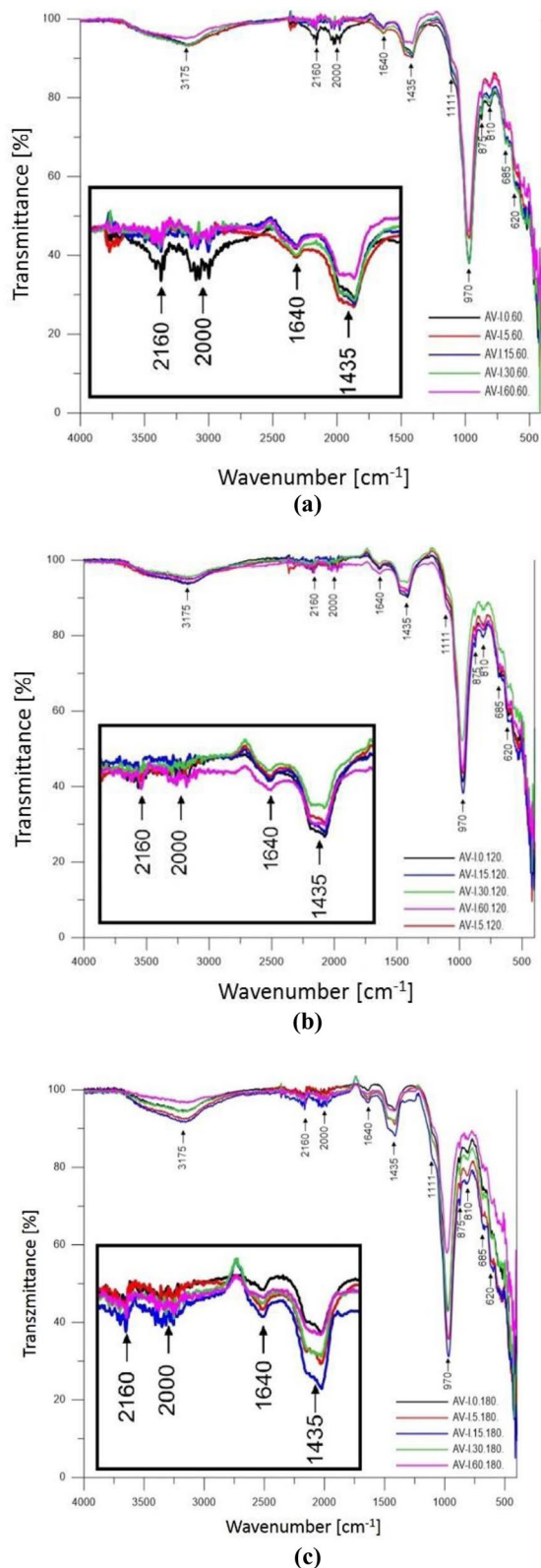


Fig. 7 FTIR spectra of the red mud sample after 60 min (a), 120 min (b), and 180 min (c) reaction time after various mechanical activation residence time

and carbonation, but due to high goethite amount the fine details related to hirschtite and cancrinite phases remain hindered. However, in the case of 180 min residence time, for the AV-I-60-180 sample there is a significant overall drop in transmittance, which is more significant for goethite water and Fe–O–Fe bands, as compared to the raw sample. The phenomenon is linked to the strong agglomeration by milling, but also amorphization process observed for this sample by XRD.

pH Measurements

The red mud suspension rapidly reacts with CO_2 in the form of carbonic acid and neutralizes the excess base in the form of NaOH , Na_2CO_3 , $\text{Al}(\text{OH})_4$. The red mud suspension rapidly reacts with CO_2 in the form of carbonic acid and neutralizes the excess base in the form of NaOH , Na_2CO_3 , $\text{Al}(\text{OH})_4$. The pH of the suspension decreased from 10 down to 6.81 the initial alkaline to a slightly acidic nature due to the weak acid in solution dissolved in the water to be absorbed, which results in the presence of the red mud coated with carbonates began to dissolve. At the end of cycle which indicated the changes of the high pH towards slightly acidic (Fig. 8). The equilibrium pH was achieved between 6.1 and 7.1 due to HCO_3^- ions. This may be the result of the solved CO_2 in water that caused the solution of some minerals of the red mud.

When the pH decreased there were some Na bearing minerals which dissolved easily such as cancrinite. The highest decrease of pH was experienced in the first reaction hour, when there was much free reaction partner for CO_2 sequestration. The pH reached the value of 6.2 meaning that it became slightly acidic. In this way it is expected that CO_2 sequestration using red mud will solve the environmental problem of red mud storage (high alkalinity). This was a result similar to that of Changming et al. [86], obtained in their measurements on red mud.

Scanning Electron Microscopy (SEM)

Figure 9a and b shows the morphological structure of red mud before and after carbonation. SEM images of the microstructure of red mud show the aggregates of fine particles about 3...5 μm size which is in correspondence with the laser particle size analysis results. It can be observed that, the original red mud was fine grained, so the individual particles cannot be seen, only in aggregates due to the drying after wet sequestration. The images indicate that significant difference in the grain size or morphology cannot be observed after CO_2 sequestration, that may be the result of surface encrusting.

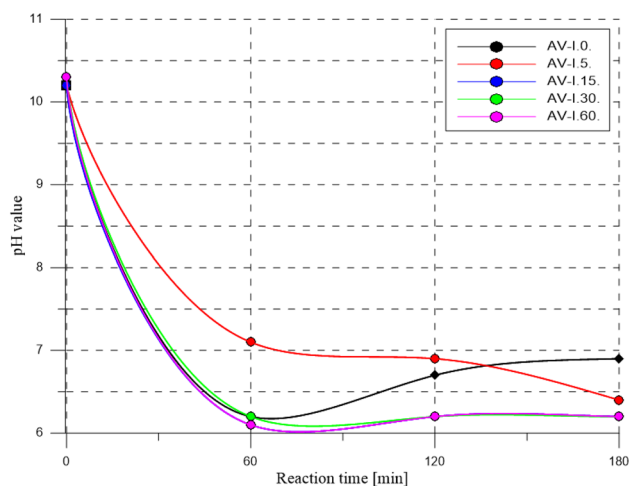


Fig. 8 Variation of pH as function of grinding time and reaction time

The EDX analysis of the red mud sample shows the presence of particular elements as shown in Table 2. The main elements observed are Fe, O, Na, Al, and Si.

The EDX measurements indicate the presence of iron as shown the XRD analyses also in the form of hematite. The Fe content ranges from 13.95 to 32.28 wt%. The untreated red mud sample has higher Na content (7.69 and 7.85 wt%) than the treated samples (1.43 ... 2.48 wt%). Oxygen content of Fig. 9b points (49.58 ... 49.82 wt%) show higher value compared to that of Fig. 9a (39.89 and 41.79 wt%), which means increasing oxygen content after CO₂ sequestration. Additionally, carbon content increased as well after red mud–CO₂ reactions indicating carbonate formation which is in correspondence with the results of X-ray diffraction and FTIR measurements.

Table 2 The result of the EDX analyses of raw and treated red mud samples

	Figure 9a		Figure 9b		
	1	2	1	2	3
O	41.79	39.89	49.58	49.61	49.82
Ca	1.79	1.76	16.88	18.64	23.03
Fe	28.58	32.28	15.81	17.60	13.95
C	–	–	6.61	5.22	5.04
Al	9.41	9.45	3.95	3.75	3.31
Na	7.85	7.69	2.78	2.18	1.43
Si	7.51	6.53	2.45	1.73	2.10
Ti	1.90	2.39	1.30	1.27	1.33
Mg	0.43	–	0.65	–	–

Conclusions

Previously, researchers' work has provided studies on the mechanical activation of red mud and CO₂ sequestration of red mud separately. However, the two synergetic process together have not yet been studied to a sufficient extent. The following conclusions can be drawn based on the results of CO₂ sequestration behavior of mechanically activated red mud:

- Mechanical activation can influence the CO₂ sequestration ability of red mud, but process parameters have to be optimized. The highest amount of CO₂ captured on the 15 min mechanically activated red mud sample with 180 min reaction time.
- Cancrinite captured CO₂ in its crystal structure as carbonate which is the main mineral phase responsible for

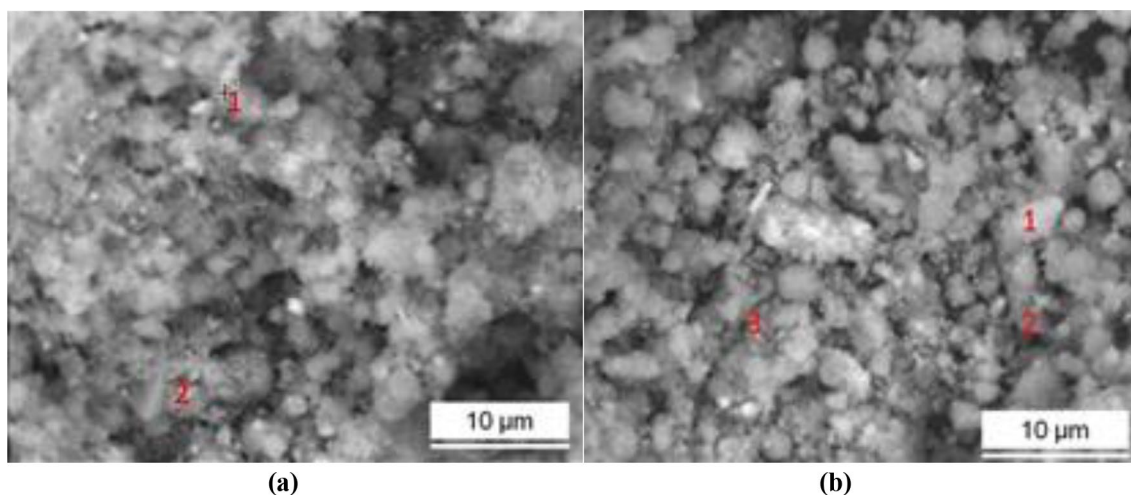


Fig. 9 The morphology of the red mud sample before (a) and after CO₂ sequestration (b)

carbonation of red mud proved by XRD. It can be stated that in the first 120 min the precipitation was the main process, which turned into dissolution after 180 min reaction time.

- The amount of captured CO₂ has a maximum point on the FTIR curves. The intensities of the carbonate band on the FTIR spectra varied due to the process of precipitation and dissolution.
- SEM EDX results indicated increased oxygen and carbon content after CO₂ sequestration.
- The pH decreased from 10 to 6 at the end of neutralization. Utilization of red mud for sequestration of CO₂ and its neutralization will reduce its environmental problem and storage area.
- The carbon-dioxide capture has multiple benefits. The residual sodium reacts with carbon dioxide while reduces the pH of the red mud. The neutralized reaction product is environmentally friendly, it is suitable for construction materials, beside the positive effect of coarsening of the carbonated particles reducing PM₁₀ and PM_{2.5}.

Acknowledgements The described article was carried out as part of the "Sustainable Raw Material Management Thematic Network—RING 2017", EFOP-3.6.2-16-2017-00010 project in the framework of the Széchenyi2020 Program. The realization of this project is supported by the European Union, co-financed by the European Social Fund. The authors express their thanks to Tibor Ferenczi senior researcher for helping in the sequestration experiments.

Funding Open access funding provided by University of Miskolc.

Open Access This article is licensed under a Creative Commons Attribution 4.0 International License, which permits use, sharing, adaptation, distribution and reproduction in any medium or format, as long as you give appropriate credit to the original author(s) and the source, provide a link to the Creative Commons licence, and indicate if changes were made. The images or other third party material in this article are included in the article's Creative Commons licence, unless indicated otherwise in a credit line to the material. If material is not included in the article's Creative Commons licence and your intended use is not permitted by statutory regulation or exceeds the permitted use, you will need to obtain permission directly from the copyright holder. To view a copy of this licence, visit <http://creativecommons.org/licenses/by/4.0/>.

References

1. Björklöf, T., Zevenhoven, R.: Energy efficiency analysis of CO₂ mineral sequestration in magnesium silicate rock using electrochemical steps. *Chem. Eng. Res. Des.* **90**(10), 1467–1472 (2012)
2. Rashid, M.I., Benhelal, E., Farhang, F., Oliver, T.K., Rayson, M.S., Brent, G.F., Stockenhuber, M., Kennedy, E.M.: Development of concurrent grinding for application in aqueous mineral carbonation. *J. Clean. Prod.* **212**, 151–161 (2019)
3. Yadav, V.S., Prasad, M., Khan, J., Amritphale, S.S., Singh, M., Raju, C.B.: Sequestration of carbon dioxide (CO₂) using red mud. *J. Hazard. Mater.* **176**(1–3), 1044–1050 (2010)
4. Rigopoulos, I., Petalidou, C.K., Vasiliades, A.M., Delimitis, A., Ioannou, I., Efstathiou, M.A., Kyratsi, T.: Carbon dioxide storage in olivine basalts: effect of ball milling process. *Powder Technol.* **273**, 220–229 (2015)
5. Lal, R.: Soil carbon sequestration impacts on global climate change and food security. *Science* **304**(5677), 1623–1627 (2009)
6. Bonenfant, D., Kharoune, L., Sauve, S., Hausler, R., Niquette, P., Mimeault, M., Kharoune, M.: CO₂ sequestration potential of steel slags at ambient pressure and temperature. *Ind. Eng. Chem. Res.* **47**(20), 7610–7616 (2008)
7. Humbert, P.S., Gomes, J.C.: CO₂ activated steel slag-based materials: a review. *J. Clean. Prod.* **208**, 448–457 (2019)
8. Montes-Hernandez, G., Perez-Lopez, R., Renard, F., Nieto, J.M., Charlet, L.: Mineral sequestration of CO₂ by aqueous carbonation of coal combustion fly-ash. *J. Hazard. Mater.* **161**(2–3), 1347–1354 (2009)
9. Meylan, F.D., Moreau, V., Erkman, S.: CO₂ utilization in the perspective of industrial ecology, an overview. *J. Carbondioxide Util.* **12**, 101–108 (2015)
10. Romão, I., Slotte, M., Gando-Ferreira, L.M., Zevenhoven, R.: CO₂ sequestration with magnesium silicates—exergetic performance assessment. *Chem. Eng. Res. Des.* **92**(12), 3072–3082 (2014)
11. Wang, F., Dreisinger, D., Jarvis, M., Hitchins, T.: Kinetics and mechanism of mineral carbonation of olivine for CO₂ sequestration. *Miner. Eng.* **131**, 185–197 (2019)
12. Jang, J.G., Kim, G.M., Kim, H.J., Lee, H.K.: Review on recent advances in CO₂ utilization and sequestration technologies in cement-based materials. *Constr. Build. Mater.* **127**, 762–773 (2016)
13. Ghacham, A.B., Pasquier, L.C., Cecchi, E., Blais, J.F., Mercier, G.: Valorization of waste concrete through CO₂ mineral carbonation: optimizing parameters and improving reactivity using concrete separation. *J. Clean. Prod.* **166**, 869–878 (2017)
14. Kaliyavaradhan, S.K., Ling, T.C.: Potential of CO₂ sequestration through construction and demolition (C & D) waste: an overview. *J. Carbondioxide Util.* **20**, 234–242 (2017)
15. Britt, D., Furukawa, H., Wang, B., Glover, T.G., Yaghi, O.M.: Highly efficient separation of carbon dioxide by a metal-organic framework replete with open metal sites. *Proc. Natl. Acad. Sci. USA.* **106**(49), 20637–20640 (2009)
16. Sahu, R.C., Patel, R.K., Ray, B.C.: Neutralization of red mud using CO₂ sequestration cycle. *J. Hazard. Mater.* **179**(1–3), 28–34 (2010)
17. Jones, G., Joshi, G., Clark, M., McConchie, D.: Carbon capture and the aluminum industry: preliminary studies. *Environ. Chem.* **3**(4), 297–303 (2006)
18. Wang, S., Ang, H.M., Tade, M.O.: Novel application of red mud as coagulant, adsorbent and catalyst for environmentally benign processes. *Chemosphere* **72**(11), 1621–1635 (2008)
19. Genc-Fuhrman, H., Tjell, J.C., McConchie, D.: Adsorption of arsenic from water using activated neutralized red mud. *Environ. Sci. Technol.* **38**(8), 2428–2434 (2004)
20. Khairul, M.A., Zanganeh, J., Moghtaderi, B.: Review The composition, recycling and utilisation of Bayer red mud. *Resour. Conserv. Recycl.* **141**, 483–498 (2019)
21. Shi, C., Xu, J., Beckman, E., Enick, R.: Carbon dioxide sequestration via pH reduction of red mud using liquid CO₂ ACS division of fuel. *Chemistry* **45**(4), 703–705 (2000)
22. Hanahan, C., McConchie, D., John, P., Creeiman, R., Clark, M., Stocksiek, C.: Chemistry of seawater neutralization of bauxite refinery residues (red mud). *Environ. Eng. Sci.* **21**(2), 125–138 (2004)
23. Amritphale, S.S., Patel, M.: Utilization of red mud, fly ash for manufacturing bricks with pyrophyllite. *Silicates Ind.* **3–4**, 31–35 (1987)

24. Vincenzo, M.S., Renz, C., Stefano, M., Giovanni, C.: Bauxite red mud in the ceramic industry. Part 2: production of clay based ceramics. *J. Eur. Ceram. Soc.* **20**(3), 245–252 (2000)
25. Yalcin, N., Sevnec, V.: Utilization of bauxite waste in ceramic glazes. *Ceram. Int.* **26**(5), 485–493 (2000)
26. Wang, W., Chen, W., Liu, H., Han, C.: Recycling of waste red mud for production of ceramic floor tile with high strength and lightweight. *J. Alloy. Compd.* **748**, 876–881 (2018)
27. Collazo, A., Fernandez, D., Izquierdo, M., Novoa, X.R., Perez, C.: Evaluation of red mud as surface treatment for carbon steel painting. *Process Organic Coat.* **52**(4), 351–358 (2005)
28. Kavas, T.: Use of boron waste as a fluxing agent in production of red mud brick. *Build. Environ.* **41**(12), 1779–1783 (2006)
29. Kehagia, F.: Construction of an unpaved road using industrial by-products (bauxite residue). *WSEAS Trans. Environ. Dev.* **10**, 2224–2496 (2014)
30. Liu, W., Yang, J., Xiao, B.: Application of Bayer red mud for iron recovery and building material production from aluminosilicate residues. *J. Hazard. Mater.* **161**(1), 474–478 (2009)
31. Pera, J., Boumaza, R., Ambroise, J.: Development of a pozzolanic pigment from red mud. *Cem. Concr. Res.* **27**(10), 1513–1522 (1997)
32. Tsakiridis, E., Agatzini-Leonardou, S., Oustadakis, P.: Red mud addition in the raw meal for the production of Portland cement clinker. *J. Hazard. Mater.* **116**(1–2), 103–110 (2004)
33. He, H., Yue, Q., Su, Y., Gao, B., Gao, Y., Wang, J., Yu, H.: Preparation and mechanism of the sintered bricks produced from Yellow River silt and red mud. *J. Hazard. Mater.* **203–204**, 53–61 (2012)
34. Ghosh, I., Guha, S., Balasubramaniam, R., Kumar, A.V.R.: Leaching of metals from fresh and sintered red mud. *J. Hazard. Mater.* **185**(2–3), 662–668 (2011)
35. Coruh, S., Ergun, O.N.: Use of fly ash, phosphogypsum and red mud as a liner material for the disposal of hazardous zinc leach residue waste. *J. Hazard. Mater.* **173**(1–3), 468–473 (2010)
36. Kalkan, E.: Utilization of red mud as a stabilization material for the preparation of clay liners. *Eng. Geol.* **87**(3–4), 220–229 (2006)
37. Gray, C.W., Dunham, S.J., Dennis, P.G., Zhao, F.J., McGrath, S.P.: Field evaluation of in situ remediation of a heavy metal contaminated soil using lime and red-mud. *Environ. Pollut.* **142**(3), 530–539 (2006)
38. Liu, Y., Naidu, R., Ming, H.: Red mud as an amendment for pollutants in solid and liquid phases review. *Geoderma* **163**(1–2), 1–12 (2011)
39. Asokan, P., Saxeian, M., Asolekar, S.R.: Coal combustion residues-environmental implications and recycling potentials. *Resour. Conserv. Recycl.* **43**(3), 239–262 (2005)
40. Kumar, A., Kumar, S.: Development of paving blocks from synergistic use of red mud and fly ash using geopolymerization. *Constr. Build. Mater.* **38**, 865–871 (2013)
41. Mucsi, G., Szabo, R., Racz, Á., Molnar, Z., Kristály, F., Kumar, S.: Influence of red mud on the properties of geopolymer derived from mechanically activated lignite fly ash. In: *Proceedings of the Bauxite Residue Valorisation and Best Practices Conference, Leuven* (2015)
42. Singh, M., Upadhyay, S.N., Prasad, P.M.: Preparation of iron rich cement from red mud. *Cem. Concr. Res.* **27**(7), 1037–1046 (1997)
43. Amritphale, S., Avneesh Anshul, S., Navin Chandra, N., Ramakrishnan, N.: A novel process for making radiopaque material using bauxite-red mud. *J. Eur. Ceram. Soc.* **27**(4), 1945–1951 (2007)
44. Mukiza, E., Zhang, L., Liu, X., Zhang, N.: Utilization of red mud in road base and subgrade materials: a review. *Resour. Conserv. Recycl.* **141**, 187–199 (2019)
45. Gupta, V.K., Ali, I., Saini, V.K.: Removal of chlorophenols from wastewater using red mud: an aluminum industry waste. *Environ. Sci. Technol.* **38**(14), 4012–4018 (2004)
46. Nadaroglu, H., Kalkan, E., Demir, N.: Removal of copper from aqueous solution using red mud. *Desalination* **251**(1–5), 90–95 (2010)
47. Altundogan, H.S., Altundogan, S., Tumen, F., Bildik, M.: Arsenic adsorption from aqueous solutions by activated red mud. *Waste Manag.* **22**(3), 357–363 (2002)
48. Cooling, D.J., Hay, P.S., Guilfoyle, L.: Carbonation of bauxite residue. In: *Proceeding of the 6th International Alumina Quality Workshop*, vol. 185, pp. 190 (2002)
49. Deihimi, N., Irannajad, M., Rezai, B.: Characterization studies of red mud modification processes as adsorbent for enhancing ferricyanide removal. *J. Environ. Manag.* **206**(15), 266–275 (2018)
50. Pulford, I.D., Hargreaves, J.S.J., Durisová, J., Kramulova, B., Girard, C., Balakrishnan, M., Batra, V.S., Rico, J.L.: Carbonised red mud—a new water treatment product made from a waste material. *J. Environ. Manag.* **100**, 59–64 (2012)
51. Apak, R., Tütem, E., Hügül, M., Jülide, H.: Heavy metal cation retention by unconventional sorbents (red muds and fly ashes). *Water Res.* **32**(2), 430–440 (1998)
52. Cengeloglu, Y., Kir, E., Ersoz, M.: Removal of fluoride from aqueous solutions using red mud. *Sep. Purif. Technol.* **28**(1), 81–86 (2002)
53. Coruh, S.: Immobilization of copper flotation water using red mud and clinoptilolite. *Waste Manag. Res.* **26**(5), 409–418 (2008)
54. Huang, W., Wang, S., Zhu, Z., Li, L., Yao, X., Rudolph, V.: Phosphate removal from wastewater using red mud. *J. Hazard. Mater.* **158**(1), 35–42 (2008)
55. Li, Y., Liu, C., Luan, Z., Peng, X., Zhu, C., Chen, Z.: Phosphate removal from aqueous solutions using raw and activated red mud and fly ash. *J. Hazard. Mater.* **137**(1), 374–383 (2006)
56. Pradhan, J., Das, S.N., Thakur, R.S.: Adsorption of hexavalent chromium from aqueous solution by using active red mud. *J. Colloid Interface Sci.* **217**(1), 137–141 (1999)
57. Santona, L., Castaldi, P., Melis, P.: Evaluation of the interaction mechanisms between red muds and heavy metals. *J. Hazard. Mater.* **136**(2), 324–329 (2006)
58. Wang, S., Boyjoo, Y., Choueib, A., Zhu, Z.H.: Removal of dyes from aqueous solution using fly ash and red mud. *Water Res.* **39**(1), 129–138 (2005)
59. Yue, Q., Zhao, Y., Li, Q., Li, W., Gao, B., Han, S.: Research on the characteristics of red mud granular adsorbents (RMGA) for phosphate removal. *J. Hazard. Mater.* **176**(1–3), 741–748 (2010)
60. Gupta, V.K., Gupta, M., Sharma, S.: Process development for the removal of lead and chromium from aqueous solutions using red mud—an aluminum industry waste. *Water Res.* **35**(5), 1125–1134 (2001)
61. Huntzinger, D.N., Gierke, J.S., Sutter, L.L., Kawatra, S.K., Eisele, T.C.: Mineral carbonation for carbon sequestration in cement kiln dust from waste piles. *J. Hazard. Mater.* **168**(1), 31–37 (2009)
62. Huijgen, W.J.J., Witkamp, J., Comans, R.N.J.: Mineral CO₂ sequestration by steel slag carbonation. *Environ. Sci. Technol.* **39**(24), 9676–9682 (2005)
63. Uibu, M., Kuusik, R., Andreas, L., Kirsimäe, K.: The CO₂-binding by Ca-Mg-silicates in direct aqueous carbonation of oil shale ash and steel slag. *Energy Procedia* **4**, 925–932 (2011)
64. Kuusik, R., Veskimäe, H., Uibu, M.: Carbon dioxide binding in the heterogeneous systems formed by combustion of oil shale 3. Transformations in the system suspension of ash—Flue gases. *Oil Shale* **19**(3), 277–288 (2002)
65. Yang, N., Liu, S., Yang, S.: Molecular simulation of preferential adsorption of CO₂ over CH₄ in Na-montmorillonite clay material. *Appl. Surf. Sci.* **356**, 1262–1271 (2015)

66. Li, J., Hitch, M.: Economic analysis on the application of mechanical activation in an integrated mineral carbonation process. *Int. Biodeterior. Biodegrad.* **128**, 63–71 (2018)
67. Li, J., Hitch, M.: Mechanical activation of magnesium silicates for mineral carbonation, a review. *Miner. Eng.* **128**, 69–83 (2018)
68. Li, J., Hitch, M.: Ultra fine grinding and mechanical activation of mine waste rock using a planetary mill for mineral carbonation. *Int. J. Miner. Process.* **158**, 18–26 (2017)
69. Reyes, C.A.R., Williams, C., Alarcón, O.M.C.: Nucleation and growth process of sodalite and cancrinite from kaolinite-rich clay under low-temperature hydrothermal conditions. *Mater. Res.* **16**(2), 424–438 (2013)
70. Deer, W.A., Howie, R.A., Wise, W.S., Zussman, J.: *Rock-Forming Minerals: Framework Silicates—Silica Minerals, Feldspathoids and Zeolites*, 2nd edn. Vol 4B, p. 982. Geological Society of London, ISBN-10: 1862391440 (2006)
71. Juhász, A.Z., Opocky, L.: Szilikátok mechanikai aktiválása finomőrléssel. Akadémia Kiadó 243 (1982)
72. Chukanov, V.N., Chervonnyi, D.A.: *Infrared Spectroscopy of Minerals and Related Compounds*. Springer ISBN 2366-1585 (2014)
73. Gotic, M., Svetzar, M.: Mössbauer FT-IR and FE SEM investigation of iron oxides precipitated from Fe₃O₄ solutions. *J. Mol. Struct.* **834–836**(27), 445–453 (2007)
74. Al Bakri-Abdullah, M.M., Hussin, K., Bnhussain, M., Ismail, K.N., Yahya, Z., Razak, R.A.: Fly ash-based geopolymer lightweight concrete using foaming agent. *Int. J. Mol. Sci.* **13**(6), 7186–7198 (2012)
75. Cudannec, Y., Lecerf, A.: The transformation of ferrihydrite into goethite or hematite, revisited. *J. Solid State Chem.* **179**(3), 716–722 (2005)
76. Chukanov, V.N., Pekov, I.V., Olysysh, V., Zubkova, N.V., Viganina, M.: Crystal chemistry of cancrinite-group minerals with an AB-type framework: a review and new data. II. IR spectroscopy and its crystal-chemical implications. *Can. Mineral.* **49**(5), 1151–1164 (2011)
77. Dodoo-Arhin, D., Konadu, D.S., Annan, E., Buabeng, F.P., Yaya, A., Agyei-Tuffour, B.: Fabrication and characterisation of ghanaiian bauxite red mud-clay composite bricks for construction applications. *Am. J. Mater. Sci.* **3**(5), 110–119 (2013)
78. Sing, S., Aswath, M.U., Ranganath, R.V.: Effect of mechanical activation of red mud on the strength of geopolymer binder. *Constr. Build. Mater.* **177**, 91–101 (2018)
79. Tóth, M.T., Schubert, F., Raucsik, B., Fintor, K.: Mineralogical and geochemical constraints of the REE accumulation in the Almásfűzitő red mud depository in Northwest Hungary. *Appl. Sci.* **9**(18), 3654 (2019)
80. Mucsi, G.: A review on mechanical activation and mechanical alloying in stirred media mill. *Chem. Eng. Res. Des.* **148**, 460–474 (2019)
81. Reddy, P.S., Reddy, N.G., Serjun, V.Z., Mohanty, B., Kumar, D.S., Reddy, K.R., Rao, B.H.: Properties and assessment of applications of red mud (bauxite residue): current status and research needs. *Waste Biomass Valoriz.* **12**, 1185–1217 (2021)
82. Young-Soo, H., Sangwoo, Ji., Pyeong-Koo, L., Chamteut, O.: Bauxite residue neutralization with simultaneous mineral carbonation using atmospheric CO₂. *J. Hazard. Mater.* **326**, 87–93 (2017)
83. Yuancheng, L., Xiaobo, M., Young, K., Degang, I., Chongjian, T.: Preparation of red mud-based geopolymer materials from MSWI fly ash and red mud by mechanical activation. *Waste Manag.* **83**, 202–208 (2019)
84. Rigopoulou, I., Petalidou, C.K., Vasiliades, A.M., Delimitis, A., Ioannou, I., Efstathiou, M.A., Kyratsia, T.: On the potential use of quarry waste material for CO₂ sequestration. *J. Carbon Dioxide Util.* **16**, 328–335 (2016)
85. Ventura, G.D., Gatta, G.D., Redhammer, G.J., Bellatreccia, F., Loose, A., Parodi, G.C.: Single-crystal polarized FTIR spectroscopy and neutron diffraction refinement of cancrinite. *Phys. Chem. Miner.* **36**, 193–206 (2009)
86. Changming, L., Hong, Z., Pingle, L., Jian, Y., Feng, G., Guangwen, X., Zhan-guo, Z.: The recycle of red mud as excellent SCR catalyst for removal of NO_x. *RSC Adv.* **7**(84), 53622–53630 (2017)
87. Chongqing, W., Xue, Z., Ruirui, S., Yijun, C.: Neutralization of red mud using bio-acid generated by hydrothermal carbonization of waste biomass for potential soil application. *J. Clean. Prod.* **271**, 122525 (2020)
88. Committee on the Science of Climate Change Division on Earth and Life Studies: National Research Council, Climate change science an analyses of some key questions, National academy press 2001 Constitution Avenue, N.W. Washington, D.C. (2001)
89. Pappu, A., Saxena, M., Asolekar, S.R.: Solid wastes generation in India and their recycling potential in building materials build. *Environment* **42**(6), 2311–2320 (2007)
90. Wouter, J.J., Huijgen, J., Witkamp, G.J., Comans, N.J.R.: Mineral CO₂ sequestration by steel slag carbonation. *Environ. Sci. Technol.* **39**(24), 9676–9682 (2005)
91. Yang, J., Xiao, B.: Development of unsintered construction materials red mud wastes produced in the sintering alumina process. *Constr. Build. Mater.* **22**(12), 2299–2307 (2008)
92. EEA 2017: Air quality in Europe — 2017 report, ISSN 1977-8449, European Environment Agency

Publisher's Note Springer Nature remains neutral with regard to jurisdictional claims in published maps and institutional affiliations.

Authors and Affiliations

Gábor Mucsi¹  · Nóra Halyag¹ · Tamás Kurusta¹ · Ferenc Kristály²

Nóra Halyag
ejtpnora@uni-miskolc.hu

Tamás Kurusta
ejttamas@uni-miskolc.hu

Ferenc Kristály
askkf@uni-miskolc.hu

¹ Faculty of Earth Science and Engineering, Institute of Raw Material Preparation and Environmental Process Engineering, University of Miskolc, Egyetemváros, Miskolc 3515, Hungary

² Faculty of Earth Science and Engineering, Institute of Mineralogy and Geology, University of Miskolc, Egyetemváros, Miskolc 3515, Hungary